

# Mass Determination Method for $\tilde{e}_{L,R}^\pm$ above Production Threshold

Mihai Dima, James Barron, Anthony Johnson, Luke Hamilton, Uriel Nauenberg, Matthew Route, David Staszak, Matthew Stolte, and Tara Turner  
*Department of Physics, University of Colorado, Boulder*

The study of the selectron decay for energies above threshold is subject to signal deconvolution difficulties and to Standard Model (SM) and Supersymmetry backgrounds, of which the largest are  $W^+W^-$  and  $\gamma^*\gamma^*$ . The important features of  $\tilde{e}_{L,R}^\pm$  production are used to design an experimentally robust method both for determining the selectron masses and for suppressing backgrounds. Additional features, such as the determination of the  $\tilde{\chi}_1^0$  mass and of the relative leptonic branching ratios of the selectron decay are present in the method.

The determination of the selectron masses using the end-points method [1] is problematic twofold: first the energy distribution of the electron and positron in the event are an overlap of 4 “box”-distributions due to the production channels  $\tilde{e}_R^+\tilde{e}_R^-$ ,  $\tilde{e}_L^+\tilde{e}_L^-$ ,  $\tilde{e}_R^+\tilde{e}_L^-$  and,  $\tilde{e}_L^+\tilde{e}_R^-$ ; second, the SUSY-signal is masked by large Standard Model (SM) backgrounds such as  $W^+W^-$  and  $\gamma^*\gamma^*$ . Even after kinematical and geometrical cuts sufficient background remains to affect the mass measurement resolution.

Many other studies of the determination of supersymmetric masses via the energy spectrum of the observed particles have been carried out [2, 3, 4] showing the usefulness of the technique and the level of accuracies possible. The selectron complication is being dealt with here.

During Snowmass’01 it was realised that the difference between the positron energy distribution and that of the electron can solve these problems and additionally offer new features, such as built in redundancy, the determination of the  $\tilde{\chi}_1^0$  mass and of the partial selectron branching ratios to  $\tilde{\chi}_1^\pm\nu$  and  $\tilde{\chi}_1^0e^\pm$ . Tangential information about the  $\tilde{\chi}_1^\pm$  and  $\tilde{\tau}_1^\pm$  masses is also available.

The  $e^+e^-$  energy distributions difference is given by:

$$\Delta(E) = Lumi \cdot (\sigma_{RL} - \sigma_{LR}) \cdot [R'_{\text{box}}(E) - L'_{\text{box}}(E)] \quad (1)$$

where  $\sigma_{LR}$  for instance is the production cross section for  $\tilde{e}_L^+\tilde{e}_R^-$ , while  $R'(E)$  and  $L'(E)$  are their “box” energy distributions each normalised to unity. The prime denotes the asymmetric boost in the reaction, due to  $M_{\tilde{e}_L} \neq M_{\tilde{e}_R}$ . In this case the values of the boosts are:

$$y'_{\tilde{e}_L} = \frac{1}{2M_{\tilde{e}_L}}\sqrt{s} + \frac{M_{\tilde{e}_L}^2 - M_{\tilde{e}_R}^2}{2M_{\tilde{e}_L}\sqrt{s}} \quad (2)$$

$$y'_{\tilde{e}_R} = \frac{1}{2M_{\tilde{e}_R}}\sqrt{s} + \frac{M_{\tilde{e}_R}^2 - M_{\tilde{e}_L}^2}{2M_{\tilde{e}_R}\sqrt{s}} \quad (3)$$

where  $s$  is the square of the center of mass energy of the collision.

One can easily show that the energy ( $E^*$ ) of the electron (positron) (from the selectron decay) in the selectron rest frame and the selectron boost can be related to the electron (positron) maximum and minimum energy by:

$$E_{e^\pm}^* = \sqrt{E_{e^\pm}(H) \cdot E_{e^\pm}(L)} \quad (4)$$

$$\lambda_{\tilde{e}} = \sqrt{\frac{E_{e^\pm}(H)}{E_{e^\pm}(L)}} \quad (5)$$

where  $\lambda_{\tilde{e}} = \gamma_{\tilde{e}} + \sqrt{\gamma_{\tilde{e}}^2 - 1}$  or  $\gamma_{\tilde{e}} = \lambda_{\tilde{e}}/2 + 1/(2\lambda_{\tilde{e}})$ . Since in the decay-CM the energy - under the same  $m_e \ll M_{L,R}$  approximation, is:

$$E_{e_{L,R}}^* \cong \frac{M_{\tilde{e}_{L,R}}^2 - M_{\tilde{\chi}_1^0}^2}{2M_{\tilde{e}_{L,R}}} \quad (6)$$

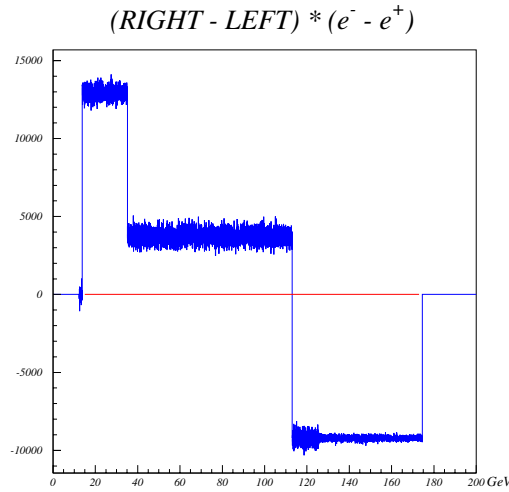


Figure 1: Energy distributions difference between the  $e^+$  and  $e^-$  distributions from selectron decays. Using the difference of the difference, between Left<sub>80%</sub> and Right<sub>80%</sub>  $e^-$  beam polarisation enhances the signal and suppresses any existing systematic differences between the positive and negative charge tracks

from these equations we can write four equations for determining the masses from boost factors and “box” energy end-points, which then lead into a final set that determines the masses [5], namely:

$$M_{\tilde{e}_R} = \frac{1}{2} \sqrt{s} \frac{\gamma'_{\tilde{e}_L} \sqrt{s} + 2E_{e_L}^*}{\gamma'_{\tilde{e}_L} \gamma'_{\tilde{e}_R} \sqrt{s} + \gamma'_{\tilde{e}_R} E_{e_L}^* + \gamma'_{\tilde{e}_L} E_{e_R}^*} \quad (7)$$

$$M_{\tilde{e}_L} = \frac{1}{2} \sqrt{s} \frac{\gamma'_{\tilde{e}_R} \sqrt{s} + 2E_{e_R}^*}{\gamma'_{\tilde{e}_L} \gamma'_{\tilde{e}_R} \sqrt{s} + \gamma'_{\tilde{e}_L} E_{e_R}^* + \gamma'_{\tilde{e}_R} E_{e_L}^*} \quad (8)$$

This solution has variations for small deviations of the “box” end-points from their nominal values. In the fit program we input a guess point for a sub-fit that estimates the guess values for  $M_{\tilde{e}_L}$ ,  $M_{\tilde{e}_R}$  and  $M_{\tilde{\chi}_1^0}$  which are fed into the main MINUIT [6] driven fit.

The properties of the above defined distribution are remarkable. First, there are only 3 (well separated) “boxes” in the energy distribution (see Figure 1).

This means that the edges can be resolved easily, as they do not overlap in any energy range. Secondly, the edge-to-particle assignments are clear, the positive part of the distribution corresponding to  $e_R^\pm$ . Thirdly, since all SM backgrounds have the same energy distribution for the visible  $e^+$  and  $e^-$ , their difference effectively cancels such signals leaving only the statistical fluctuation of the backgrounds. Even if there is a detector asymmetry between positive and negative tracks, this can be eliminated through the use of the polarised version of the above difference:

$$\Delta\Delta(E) = (\text{Right}_{80\%} - \text{Left}_{80\%}) \cdot (e^+ e^-) \quad (9)$$

where Right<sub>80%</sub> and Left<sub>80%</sub> denote polarised  $e^-$  beam, Figure 1. In principle there is no non-supersymmetric background (physics, or machine related, such as detector, hot electronics, accelerator, etc.) that remains after this difference is performed. In addition, including polarization enhances the difference sharpening the edge of the boxes.

A large fraction of SM backgrounds can be removed by kinematical and geometrical cuts. For instance it has been shown elsewhere [7] that the  $\gamma^* \gamma^*$  background can be reduced substantially using various kinematical and geometrical cuts in the very forward direction. However, these cuts are not as effective when  $\tilde{e}_{L,R}^\pm$  and  $\tilde{\chi}_1^0$  are close in mass. Hence, this new method substantially increases our ability to detect such signals since this background should be removed when one looks at differences in the energy spectra.

For the cases analyzed in Snowmass01 this method is complicated slightly by the fact that  $\tilde{e}_L^\pm$  has two leptonic decay channels, one involving the channel  $\tilde{\chi}_1^\pm \nu$ , where the  $e^\pm$  appears as a result

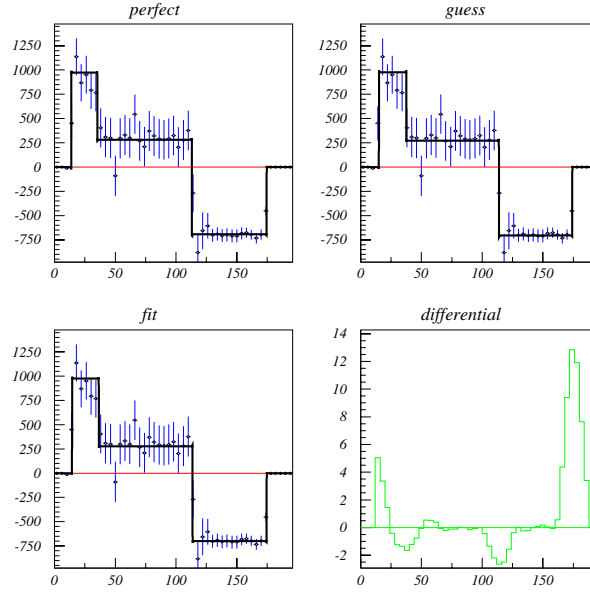


Figure 2: Fit to the  $e^+e^-$  distribution. The fit identifies the edges with a  $\sigma$ -normalised differential (lower right plot)—the results with these guess values shown in the upper right plot. The fit then proceeds to identify the best parameter combination: lower left, which can be directly compared with the upper left plot that uses the input masses.

of second and third level decay chains and one  $\tilde{\chi}_1^0 e^\pm$  where the  $e^\pm$  comes from the initial decay. In both channels the final signal is an electron and positron. In this case, which is the one we present here, the difference distribution becomes:

$$\Delta(E) = Lumi \cdot (\sigma_{RL} - \sigma_{LR}) \cdot (f + f') \cdot \left[ R'_{box}(E) - \frac{f}{f + f'} L'_{box}(E) - \frac{f'}{f + f'} X'_{box}(E) \right] \quad (10)$$

where  $X'(E)$  is the energy distribution of the visible  $e^\pm$  from the  $\tilde{\chi}_1^\pm$  decay, and  $f$  and  $f'$  are the branching fractions to  $L'(E)$  and  $X'(E)$  respectively. The power of the method in its initial form is that this histogram has to be normalised to zero, and hence any pedestal can be determined and subtracted. Overall there are only 3 free parameters in the fit:  $M_{\tilde{e}_L}$ ,  $M_{\tilde{e}_R}$  and  $M_{\tilde{\chi}_1^0}$ . This provides a very robust fit (Figure 2). In the present case the  $X'(E)$  (Figure 3) distribution has to be parametrised, and this adds one extra parameters to the fit.

The chosen model was an exponential shape for  $X'(E)$ , as determined by Monte Carlo. The general idea of the simple fit remains: a robust fit (Figure 4) with few, tightly bound parameters. The fit yields also the  $f/(f + f')$  and  $f'/(f + f')$  relative leptonic branching fractions associated with  $\tilde{\chi}_1^\pm \nu$  and  $\tilde{\chi}_1^0 e^\pm$ . The  $X'(E)$  shape parameter gives general information about the  $\tilde{\chi}_1^\pm$  and  $\tilde{\tau}_1^\pm$  masses.

We carried out an analysis to determine how the errors scale with luminosity. The errors in mass determination *versus* luminosity are shown in Figure 5 for the “idealistic” case with no  $\tilde{\chi}_1^\pm \nu$  decay channel, as well for the “realistic” case with the background from such a decay chain.

An indication of saturation of the mass-errors with luminosity is shown in these plots; the luminosity at which the error reaches its limiting value occurs in the range of  $1000 \text{ fb}^{-1}$ . Increasing the luminosity may not substantially improve the mass resolution. It can be seen that the largest difference in mass-errors between the “ideal” and “real” case is for  $M_{\tilde{e}_R}$  due to its corresponding energy-“box” neighboring the perturbing  $X'(E)$  distribution.

The method presented here is a version of the end-points mass determination method, in which the visible particles’ spectra are subtracted ( $e^+e^-$ ). This eliminates the difficulties in resolving

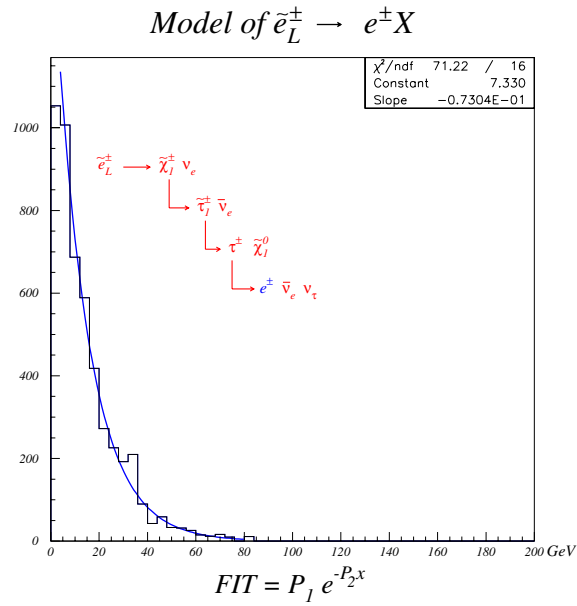


Figure 3: Parametrisation of the leptonic decays of the  $\tilde{\chi}_1^\pm$ . We show here the chosen model, an exponential, which requires only one shape parameter.

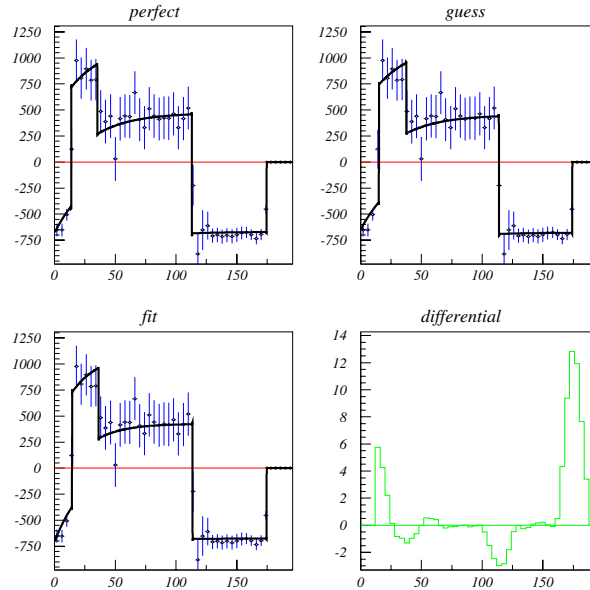


Figure 4: Fit to the distribution including the  $\tilde{\chi}_1^\pm$  mode. The influence of the latter is the negative lower energy piece. This is parametrised as an exponential and requires one extra parameter. The robustness of the fit is the same. The data presented here is for a luminosity of  $200 \text{ fb}^{-1}$ . For the input masses (in GeV)  $M_{\tilde{e}_L} = 202.1$ ,  $M_{\tilde{e}_R} = 143.0$ ,  $M_{\tilde{\chi}_1^0} = 95.7$  this fit gives  $204.0 \pm 3.1$ ,  $143.8 \pm 1.0$ ,  $96.3 \pm 0.6$  respectively.

overlapping edges at low energies, and in edge assignments which are ambiguous. The method takes into account the selectron decay involving the  $\tilde{\chi}_1^\pm \nu$  channel which has similar event signature, but an exponentially decaying energy distribution. The constraints of the problem are used as fit advantage in determining normalisations and limiting the number of free parameters ( $M_{\tilde{e}_L}$ ,  $M_{\tilde{e}_R}$ ,  $M_{\tilde{\chi}_1^0}$ , and a shape parameter for the decay mode involving the  $\tilde{\chi}_1^\pm$ ). The fit is very robust and

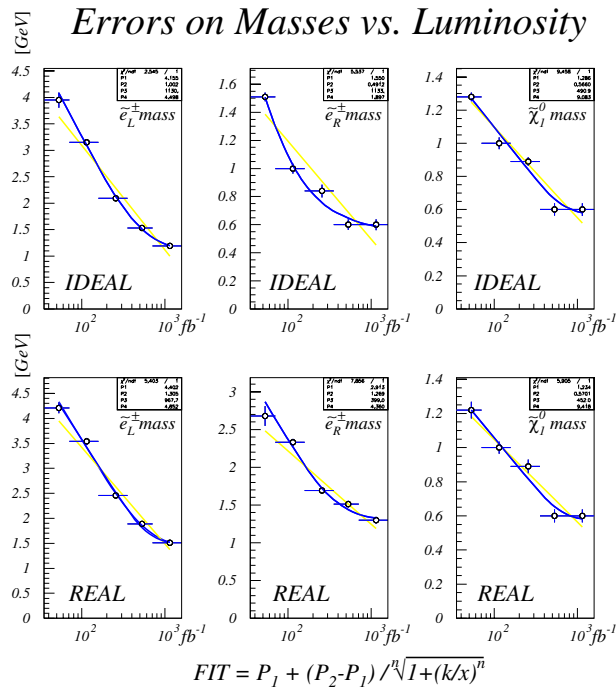


Figure 5: Mass determination errors *versus* luminosity, for the “idealistic” distribution (only  $\tilde{\chi}_1^0$ ) and for the realistic one including also the  $\tilde{\chi}_1^\pm$ . An indication of saturation with luminosity is seen which indicates the value at which 80% of the saturation limit is reached.

stable, determining not only the masses involved, but also the relative leptonic branching ratios, and some additional information about the  $\tilde{\chi}_1^\pm$  and  $\tilde{\tau}_1^\pm$  masses. A study of the mass determination errors *versus* luminosity indicates a possible saturation of the errors, as determined by the  $1/\sqrt{N}$  statistical dependence, at the level obtained for luminosities of the order of  $1000 \text{ fb}^{-1}$ .

## References

- [1] Toshifumi Tsukamoto, Keisuke Fujii, Hitoshi Murayama, Masahiro Yamaguchi, and Yasuhiro Okada, “Precision Study of Supersymmetry at Future  $e^+e^-$  Colliders,” Phys. Rev D 51, 3153 (1995).
- [2] “Supersymmetry, Chapter 3 of TESLA TDR”, DESY-2001-011, ECFA-2001-209.
- [3] H. Baer, R. Munroe and X. Tata, “Supersymmetry studies at future linear  $e^+e^-$  colliders,” Phys. Rev. D 54, 6735 (1996) [hep-ph/9606325].
- [4] The various studies by the Colorado group are discussed in <http://hep-www.colorado.edu/SUSY>.
- [5] A full PRL article is being prepared to present the analysis in detail.
- [6] MINUIT v94.1 minimisation program, F.James, F.Roos, CERN (1967).
- [7] Colorado Group, SUSY- $\tilde{e}^\pm/\tilde{\mu}^\pm$  Studies, LCWS-2000 Proceedings, Fermilab, October 2000.